Influence of salinity on the behaviour of frozen soils

Author 1

- Nico Molls, M.Sc.
- Chair of Geotechnical Engineering and Institute of Geomechanics and Underground Technology, RWTH Aachen University, Aachen, Germany.
- ORCID number: 0009-0008-4480-4795
- e-mail: molls@gut.rwth-aachen.de
- phone: +49 241 80 2525 8

Author 2

- Raul Fuentes, Univ.-Prof. Dr.
- Chair of Geotechnical Engineering and Institute of Geomechanics and Underground Technology, RWTH Aachen University, Aachen, Germany
- ORCID number: 0000-0001-8617-7381
- e-mail: raul.fuentes@gut.rwth-aachen.de
- phone: +49 241 80 2524 7

Abstract

Salinity strongly affects the freezing and mechanical behaviour of soils, but systematic studies combining thermodynamic interpretation with strength testing are limited. This study examines the influence of NaCl on the freezing process and unconfined compressive strength of saturated sands. Freezing curves were recorded at –10 °C and –25 °C, and unfrozen water content was measured using nuclear magnetic resonance (NMR). Results show that increasing salinity lowers both the supercooling temperature and the equilibrium freezing point in accordance with the NaCl–H_2O phase diagram. At –25 °C, a second plateau in the freezing curves was observed, reflecting eutectic solidification of residual brine. Even small salt additions caused disproportionate strength reductions: at –10 °C, 0.5% NaCl reduced strength to about one-quarter of the salt-free value. At eutectic conditions, strength partially recovered as brine solidified, though the ice–soil skeleton incorporated salt crystals, producing a response distinct from fresh water soils. NMR tests confirmed a near-linear increase of unfrozen water with salinity, while the strength–liquid relation was strongly nonlinear. The novelty of this work lies in combining freezing curve analysis with direct strength testing of saline sands.

Keywords chosen from ICE Publishing list

Ground freezing; temperature effects; thermal behaviour; testing & evaluation; Strength & testing of materials; Sands; NMR relaxometry; Cold/Arctic region geotechnics; Coastal engineering

1 Introduction

The presence of dissolved salts profoundly modifies the freezing behaviour of soils. Salts not only depress the equilibrium freezing point (Atkins, 1996; Haghighi et al., 2008) through colligative and osmotic effects but also alter the soil freezing characteristic curve (SFCC), increase the fraction of unfrozen water retained at subzero temperatures, and influence ice segregation, salt migration, and cryo-concentration during freezing (Banin & Anderson, 1974; Zhou et al., 2018; Amankwah et al., 2021; Luo et al., 2023). Understanding soil freezing under saline conditions is essential for two major contexts:

1. Artificial ground freezing (AGF), widely used for temporary ground support in urban tunnelling, shaft sinking, and cross-passage construction. Here, groundwater salinity can significantly delay or complicate soil freezing. For example, during the construction of cross-passages of the Port Said tunnels beneath the Suez Canal, groundwater salinities of ~3.8% NaCl required substantially lower refrigeration temperatures than anticipated (Orth et al., 2021; Rizos et al., 2022).
2. Permafrost regions, where naturally saline soils or anthropogenic inputs (e.g., drilling muds, industrial brines, landfill leachates) modify thawing and refreezing behaviour, with implications for climate-driven permafrost degradation (Wan et al., 2015; Ying et al., 2025).

While it is well known that salts reduce the freezing point of pore water, the consequences for the mechanical strength of frozen soils remain less systematically investigated. The soil's load-bearing capacity depends largely on the volume and microstructure of the ice phase. At subzero temperatures above the eutectic point of a salt solution, a significant proportion of pore brine remains unfrozen, which weakens the ice–soil matrix (Arenson & Sego, 2004; Tilston et al., 2010). Conversely, once the eutectic temperature is crossed, the residual brine solidifies in a second freezing stage, resulting in a distinct strengthening mechanism (Journaux et al*., 2023*; Gao et al., 2024).

A further complication is that different salts produce markedly different freezing point depressions and precipitation behaviours. For instance, NaCl brine has a eutectic temperature of –21.15 °C, whereas divalent salts have lower temperatures (Loomis, 1896; Wan et al., 2021). Moreover, salt precipitation during freezing may introduce discontinuities or temperature jumps that influence the unfrozen water content and hence mechanical response (Ying et al., 2025).

Despite extensive thermodynamic studies of saline freezing processes, relatively few experimental investigations directly link salinity, freezing curves, and soil strength in a controlled laboratory setting. This gap is particularly relevant for coarse-grained soils where pore-size effects are minimized, allowing clearer isolation of salinity-driven phenomena (Xiao et al., 2018). The present study addresses this gap by systematically testing narrow-graded sand specimens saturated with NaCl solutions of varying concentrations. Freezing curves were recorded, and unconfined compression tests were performed at two subzero temperatures (–10 °C and –25 °C) to evaluate how salinity affects both the freezing process and the mechanical strength of frozen soil.

Additionally, while earlier works have described freezing point depression and unfrozen water retention in saline soils, few studies combine phase diagram–based interpretation with direct mechanical testing on frozen saline sands. The results provide new insights into how even small salt contents dramatically reduce strength at moderate subzero temperatures, while complete freezing at eutectic conditions alters the ice–soil matrix in a fundamentally different way. These findings have direct implications for the design and safety assessment of saline ground freezing projects and for predicting the mechanical response of saline permafrost.

2 Literature review

Salts influence the freezing of soils primarily by altering the thermodynamic properties of pore water and secondarily by modifying the microstructural arrangement of ice and brine.

These effects can be described using classical phase diagrams, complemented by pore-scale observations and constitutive modelling.

2.1 Freezing point depression and water activity

When a salt crystal such as NaCl dissolves in water, hydration shells form around the ions. These hydration complexes disrupt the hydrogen-bond network of liquid water, lowering the chemical potential of the system and thereby decreasing the freezing temperature (Atkins, 1996). The reduction in free energy is also expressed as a decrease in water activity, which is nearly linear with increasing NaCl concentration (Banin & Anderson, 1974; Haghighi et al., 2008). Wan et al. (2021) further showed that for Na_2SO_4, the relationship is nonlinear: water activity decreases at low concentrations, but above ~0.4 mol/L it remains nearly constant despite higher concentrations.

As already shown, the extent of freezing point depression depends strongly on the type of salt. Loomis (1896) classified electrolytes into two groups: monovalent salts such as NaCl and KCl, which produce relatively moderate freezing point depression, and divalent salts such as $MgCl_2$ or Na_2SO_4, which can cause much stronger depressions. For example, a 20% NaCl solution freezes at about –17 °C, while a 20% $MgCl_2$ solution can depress freezing to nearly –30 °C. This strong ion-specific effect is consistent with more recent experimental results (Wan et al., 2015; Wan et al., 2021).

2.2 Eutectic mixtures and two-stage freezing

The freezing process of saline water is best understood using phase diagrams. Figure **1** illustrates the NaCl–H_2O phase diagram. The eutectic composition is reached at 23.3% NaCl and 76.7% H_2O, at which the entire solution freezes at –21.15 °C. This is the lowest possible freezing point for the NaCl–H_2O system.

Above the eutectic temperature, freezing occurs in two stages. Initially, relatively pure water freezes, forming ice crystals and leaving behind a more saline brine. As cooling continues, the brine becomes increasingly concentrated, and its freezing temperature decreases further.

Eventually, when the eutectic concentration and temperature are reached, the brine itself solidifies into a mixture of ice and salt crystals (Atkins, 1996; Banin & Anderson, 1974). If the initial solution is already saturated, solid NaCl crystals are expelled during cooling until the eutectic mixture is reached. At the eutectic temperature, simultaneous crystallization of ice and brine occurs. This two-stage freezing explains the persistence of liquid brine at moderate subzero temperatures (e.g., –10 °C) and its eventual disappearance once the eutectic point is crossed (Ying et al., 2025).

During this procedure various kinds of crystal structures will form. We will concentrate here on the left hand side of the diagram where the salt is fully dissolved in a solution (i.e., for salt concentrations lower than 27.6%, beyond which the solution is regardless of the temperature supersaturated and salt crystals precipitate). The common form of pure water ice is a hexagonal crystal structure in which water molecules are arranged tetrahedrally in hydrogen bonds – called Ice Ih in Figure 1. Depending on temperature and pressure also the sodium chloride hydrate crystals build up differently. At a pressure of 1 bar there are two species of NaCl hydrates that are relevant in the context of this research. Sodium chloride dihydrate $NaCl\text{-}2H_2O$ (SC2) forms at locations where the temperature is lowered from 0 °C to the eutectic temperature of -21.15 °C and the NaCl content lies above 23.3 %. Brine crystallises as disodium chloride decaheptahydrate $2NaCl\text{-}17H_2O$ (SC8.5) at temperatures below -38.15 °C for these salt concentrations. Different pores will have different salt concentrations due to salt migration through diffusion and hence, depending on the NaCl concentration there will be pure Water ice (Ice Ih) co-existing with SC8.5, or SC8.5 with SC2 (Journaux et al., 2023). This affects thermodynamic aspects as well as the mechanical properties of the soil.

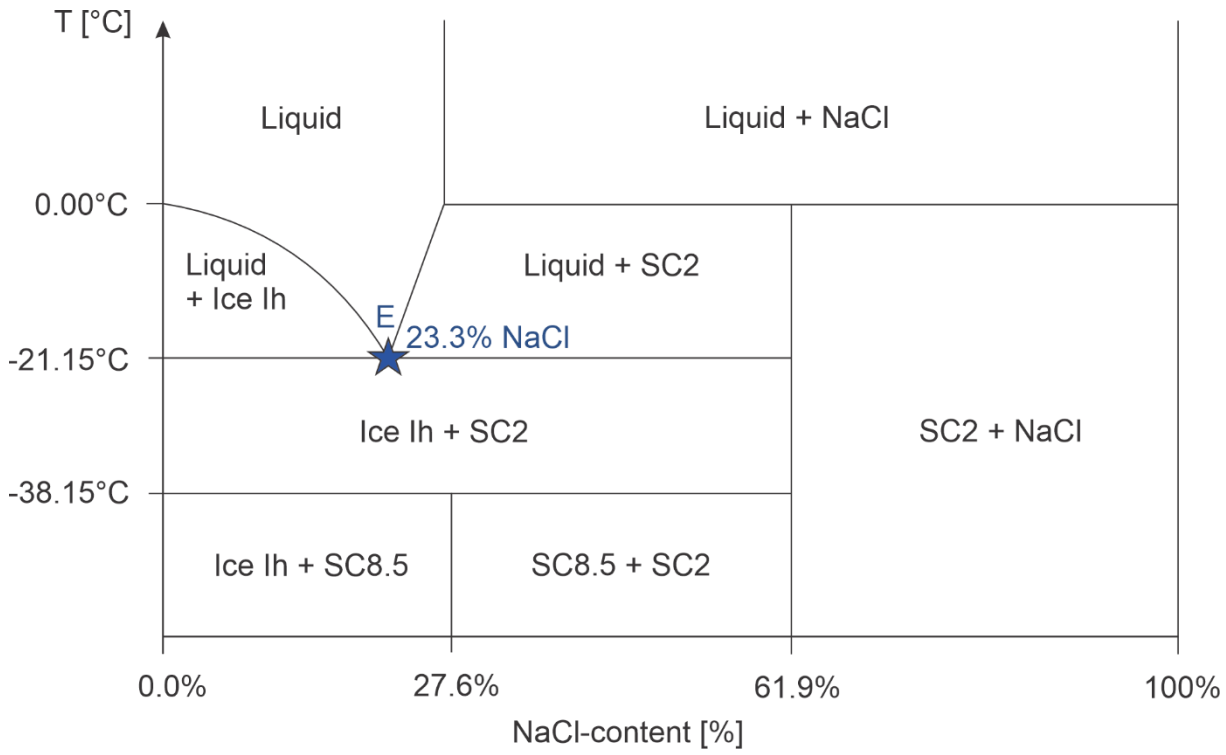

Fig. 1. H_2O-NaCl phase diagram at 1 bar. The blue star shows the eutectic point (E) (after Journaux et al., 2023)

2.3 Pore-scale processes and microstructure

In saline soils, the freezing behaviour is further complicated by pore-scale processes. As water freezes, ice initially forms in larger pores, while capillary and adsorptive forces delay freezing in finer pores due to a lowering of the so-called ice entry point (Andersland & Ladanyi, 2004). In saline soils, this size-dependent freezing is combined with solute redistribution. For example, Na_2SO_4 solutions may crystallize within pores, partially blocking them and altering the effective pore size distribution (Wan et al., 2015). This mechanism further decreases the freezing point due to enhanced adhesive forces in narrower pores. Arenson & Sego (2004) visualized freezing in coarse sands with fluorescent tracers. Their microstructural observations revealed that increasing salinity increases the amount of unfrozen pore liquid and promotes the formation of interconnected brine channels. These concentrated brine pathways, in turn, influence ice crystal morphology: instead of forming continuous ice, saline freezing often produces fragile “ice needles” emanating from mineral grains, which significantly reduces the mechanical stability of the frozen soil.

More recent studies using micro-CT imaging have confirmed that saline sands can retain continuous liquid bodies up to the eutectic temperature (Gao et al., 2024). The cooling rate also plays a critical role: rapid freezing traps brine in continuous networks, maintaining higher permeability, while slow freezing promotes brine segregation into disconnected pockets (Wang et al., 2023). This duality is particularly relevant for engineering applications such as artificial ground freezing, where the rate of freezing is controlled by the applied thermal gradient.

2.4 Thermal and mechanical implications

The influence of salts extends beyond freezing temperature. Salinity also affects thermal properties and, ultimately, soil strength. Laboratory tests show that chloride salts reduce thermal conductivity by ~0.11 $W \cdot m^{-1} \cdot K^{-1}$, whereas sulfate salts reduce it by ~0.07 $W \cdot m^{-1} \cdot K^{-1}$ (Ju et al., 2023).

The unfrozen water content (UWC) plays a central role in strength development: higher salinity results in more unfrozen water at a given temperature, leading to weaker ice–soil bonding (Watanabe & Mizoguchi, 2002; Tilston et al., 2010). Conversely, once the eutectic temperature is reached and residual brine solidifies, the ice–soil matrix regains continuity, though salt crystals are incorporated into the structure. This transition results in a different form of mechanical stabilization that is not observed in fresh water soils (Amankwah et al., 2021; Luo et al., 2023).

The sequence of freezing in soils can also be represented by a cooling curve. Figure **2** illustrates this process: after an initial supercooling (T_{SC}), ice nucleation releases latent heat, stabilizing the temperature at the freezing point (T_f). Larger pores freeze first, followed by smaller pores as temperature decreases further. Adhesive forces in the finest pores may prevent complete freezing, leaving residual unfrozen water. In saline soils, this residual fraction is significantly larger due to solute-induced freezing point depression, explaining why brine can persist at temperatures as low as –10 °C (Andersland & Ladanyi, 2004; Wan et al., 2015; Luo et al., 2023).

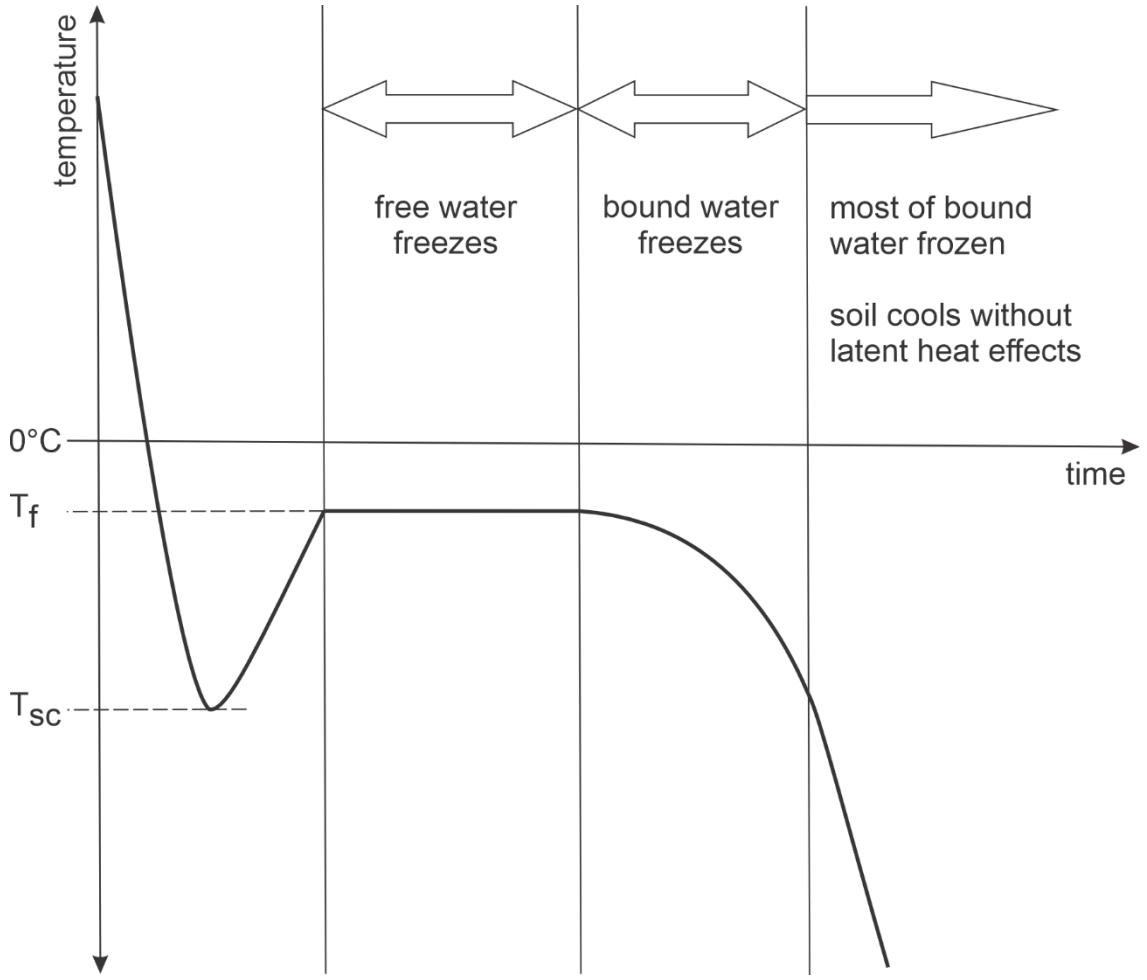

Fig. 2. Cooling curve for soil water and ice (after Andersland & Ladanyi, 2004)

2.5 Constitutive modelling of saline soil freezing

The generalized Clapeyron equation (GCE) provides the thermodynamic foundation for describing soil freezing, linking water potential, temperature, and ice–water equilibrium. In its traditional form, the GCE includes only matric potential. For saline soils, however, osmotic potential must be added to capture freezing point depression and UWC behaviour (Luo et al., 2023; Wan et al., 2024). Yet even this modification may underpredict freezing depression at higher salinities, where salt exclusion and precipitation must also be accounted for (Amankwah et al., 2021). Recent models explicitly incorporating these mechanisms provide significantly better fits to both laboratory and field SFCC data.

3 Methodology

3.1 Material and sample preparation

Narrowly graded sand with particle sizes between 0.5 mm and 1.0 mm was selected for the experiments. The use of coarse-grained material avoids pore-size freezing effects that typically occur when pore diameters are smaller than 1 µm (Watanabe & Mizoguchi, 2002; Xiao et al., 2018). For this reason, the observed freezing point depression in the present study can be attributed primarily to salinity rather than pore geometry.

Sodium chloride (NaCl) was chosen as the solute. Unlike salts such as Na_2SO_4, which may precipitate and alter pore structures, NaCl remains dissolved until the eutectic point is reached, making it suitable for isolating the thermodynamic effects of salinity (Wan et al., 2015).

Cylindrical specimens with a diameter of 50 mm and a height of 100 mm were prepared for freezing curve measurements and unconfined compression testing. This 1:2 height-to-diameter ratio follows established practice for frozen soil testing (Andersland & Ladanyi, 2004). Specimens were cast in cylindrical polyurethane (PU) moulds with a base containing a lead-through for insertion of a temperature sensor.

To ensure full saturation, specimens were prepared under saline water. The required amount of NaCl solution was first poured into the mould, and the sand was then placed in four layers, each lightly compacted. This underwater preparation minimized entrapped air, yielding degrees of saturation *Sr* between 0.95 and 1.0. Homogeneity of the method was verified by cutting frozen specimens into horizontal layers and determining density and water content by oven drying.

The NaCl solution concentrations ranged from 0.0% (distilled water) to 10.0% by mass. For example, a solution of 3.5% NaCl corresponds to 35 g NaCl per 1000 g of solution. After preparation, specimens were frozen for 24 h in the freezing laboratory chamber.

To account for the ~8% volumetric expansion of water upon freezing, moulds were left open at the top, allowing excess pore water to escape. This prevented cracking or specimen

193 distortion. After freezing, any excess ice lens formed at the specimen top was carefully
194 removed to achieve uniform dimensions of 100 mm in height.
195

196 **3.2 Experimental setup and execution**

197 Experiments were performed in the controlled freezing laboratory at GUT, where ambient
198 temperatures between –4 °C and –30 °C can be maintained with ±0.5 °C accuracy.
199 Specimens remained inside the laboratory throughout preparation, freezing, and testing,
200 ensuring no thermal disturbance.
201 Temperature control and gradients were carefully monitored. For freezing-curve specimens,
202 a PT100 probe was placed at mid-height. Temperature was logged at 1-second intervals
203 during freezing. In unconfined compression specimens, additional probes were installed at
204 the top and base, enabling assessment of axial gradients. Before testing, specimens were
205 considered at steady state when the temperature difference between top, middle, and base
206 did not exceed 0.3 °C for at least one hour. All PT100 sensors were factory-calibrated (±0.1
207 °C accuracy) and cross-checked in an ice–water bath prior to the test series. Typical
208 gradients at failure were <0.5 °C across the 100 mm specimen height.
209 Unconfined compression tests were performed at constant strain rate on specimens frozen
210 for at least 24 h. This ensured that all specimens had completed their primary freezing
211 process (see freezing curves, Section 4). The strain rate was 0.1%/min, consistent with the
212 recommendations of Andersland & Ladanyi (2004) for frozen soils at moderately low
213 temperatures. A lower rate was chosen (rather than 1.0%/min) to account for the expected
214 presence of unfrozen brine at –10 °C, which could otherwise bias failure modes. Tests were
215 terminated at 20% axial strain.
216 Axial deformation was measured with linear variable displacement transducers (LVDTs),
217 while load was recorded with a 2-ton load cell. For the reference samples (0% NaCl), a 10-
218 ton load cell was used due to their higher strength. The LVDTs have an accuracy of < ±0.05
219 mm, both load cells have an accuracy of < ±0.5 % of nominal load. Temperatures at the
220 specimen base, top, and core were recorded continuously during loading.

221

222 # 4 Experimental results

223 ## 4.1 Soil freezing curves

224 ### 4.1.1 Soil freezing curves at -10 °C

225 At an ambient temperature of –10 °C, which is above the eutectic temperature of NaCl (–
226 21.15 °C), freezing occurs in the two-stage manner described earlier. Figure **3** presents the
227 freezing curves of specimens with different NaCl concentrations.
228 For the reference sample with 0.0% NaCl, the classic freezing curve shape is observed: after
229 supercooling to –0.7 °C (T_{SC}), crystallization initiates, releasing latent heat and stabilizing the
230 temperature at the freezing point T_f = –0.1 °C for approximately 3.5 hours. Once this plateau
231 ends, the temperature gradually decreases to –3.0 °C over one hour, most likely reflecting
232 the freezing of bound water. Subsequently, the specimen cools rapidly to the ambient
233 temperature.
234 With increasing NaCl content, three systematic effects are evident:

235 1. Both the supercooling temperature (T_{SC}) and freezing temperature (T_f) decrease.
236 2. The duration of the steady freezing plateau shortens, implying that less ice forms and
237 a larger fraction of brine remains unfrozen.
238 3. The cooling rate slows, such that specimens with higher salinity require longer to
239 reach the ambient temperature. This is attributed to ongoing separation of pure water
240 from the brine during cooling, which then freezes and releases latent heat (Banin &
241 Anderson, 1974; Wan et al., 2015).

242

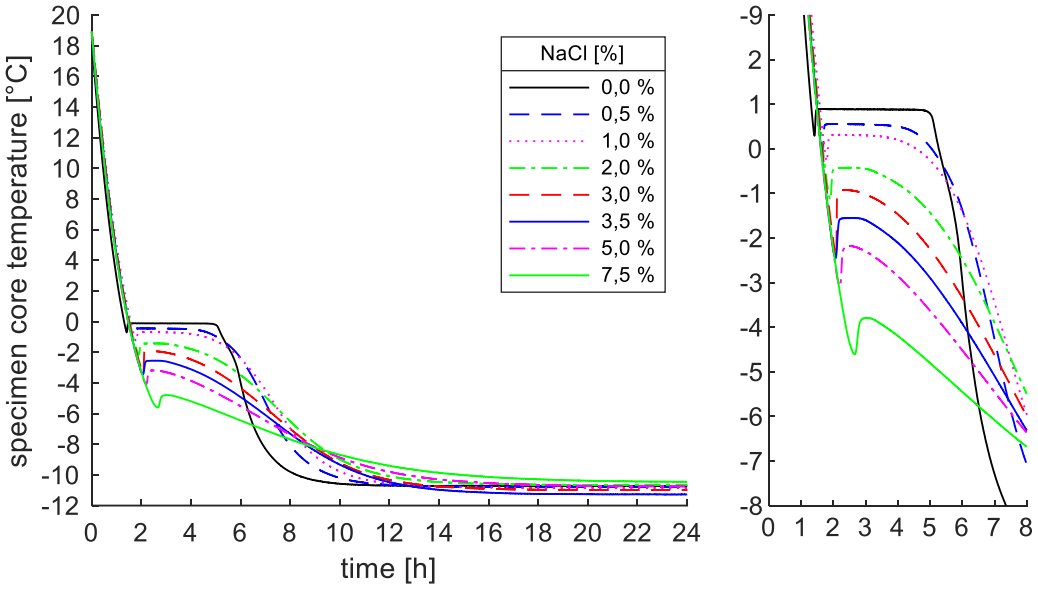

Fig. 3. Freezing curves of specimen with varying NaCl-contends at -10 °C with detail (right)

4.1.2 Soil freezing curves at -25 °C

When ambient temperature is lowered to –25 °C, below the eutectic point of NaCl, complete freezing of all specimens is achieved. Figure **4** shows the cooling curves at –25 °C. Initially, cooling occurs more rapidly than at –10 °C due to the larger temperature gradient. As a result, the supercooling (T_{SC}) and freezing (T_f) stages occur earlier in time. However, differences in T_f values are observed: at –25 °C, the higher cooling rate gives less time for brine segregation, so less pure ice forms and less latent heat is released, lowering the effective freezing temperature (Gao et al., 2024; Wang et al., 2023).

The duration of the first freezing plateau is shorter than at –10 °C, reflecting faster kinetics and reduced ice formation. After this stage, specimen core temperatures decline towards –23 to –24 °C. At this point, samples with NaCl content show a second temperature plateau, indicating a second freezing phase. This phase corresponds to the crystallization of the remaining eutectic brine, consistent with the NaCl–H_2O phase diagram (Figure **1**).

The duration of this second plateau increases disproportionately for salinities above 5%. For example, specimens with 7.5% and 10% NaCl require much longer to complete eutectic freezing, though the incremental difference between them is small. This behaviour confirms

that once a threshold salinity is reached, freezing of the residual brine becomes a slower process governed by salt precipitation kinetics (Ying et al., 2025).

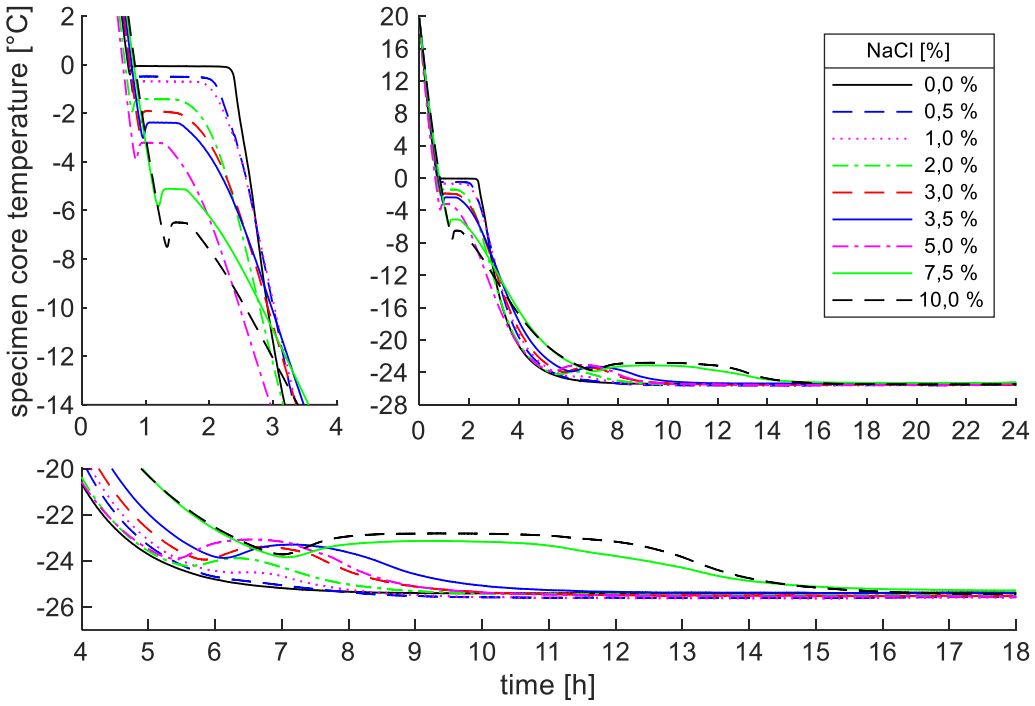

Fig. 4. Freezing curves of specimen with varying NaCl-contends at -25 °C with details (left and below)

4.1.3 Simple 1D verification.

A simple one-dimensional heat-transfer estimate confirms that the observed plateau durations are physically consistent and provides a simple means for prediction. The specimens (Ø 50 mm × 100 mm) had a volume of 1.96×10^{-4} m^3 and a surface area of 1.96×10^{-2} m^2, giving a characteristic length of ~0.01 m. The associated sensible-cooling time constant is 0.9–1.8 h, consistent with the non-plateau portions of the curves. Plateau durations are then governed by latent heat release:

$$t_L = \frac{m_w L \, \Delta\theta_i(T,S)}{hA \, \Delta T_{\text{eff}}},$$

where m_w is the specimen water mass, L the latent heat of fusion, and $\Delta\theta_i(T,S)$ the ice fraction formed at temperature T and salinity S. The ice fraction was taken from the NMR-measured liquid water contents. At –10 °C, liquid fractions increased nearly linearly with salinity, from ~0.05 (0% NaCl) to ~0.80 (10% NaCl). Using $m_w = 0.069$ kg, $L = 333.7$kJ kg^{-1}, $A = 0.0196$m², $\Delta T_{\text{eff}} \approx 10$K and two different convective coefficients: one for no salt, $h_{Sand,Water} = 9.0$ W m^{-2} K^{-1}, and one for the salty soils of $h_{Sand,Brine} = 35.0$ W m^{-2} K^{-1}, the predicted plateau durations agree well with the freezing curves (Table **1**). These convective coefficients are back-calculated and represent two effective overall surface coefficients. However, the fact that a single coefficient provides a good estimate for all salty cases supports this lumped approach as a rough estimate. Additionally, with a thermal conductivity of frozen sand $k \approx 1.7$ W m^{-1}K^{-1}and the convective coefficients (Incropera et al., 2007), the Biot number is $\ll 0.1$ for the lower coefficient justifying a lumped-capacity approach, although it is only marginal for the brine.

Table 1. Predicted vs. observed plateau durations at –10 °C

NaCl content [% by mass]	Liquid pore water due NMR [% by vol]	Predicted plateau duration [h]	Observed plateau duration [h]
0.0	0.91	3.59	~3.5
2.0	13.06	0.81	~0.8
3.5	24.87	0.70	~0.7
7.5	58.11	0.39	~0.4
10.0	78.29	0.20	~0.2

At –25 °C, the first freezing stage is accelerated by the larger temperature gradient, but a second plateau appears near –21 °C due to eutectic freezing of residual brine. This can be described by the same expression, with $\Delta\theta_i$ representing the remaining brine fraction and ΔT_{eff} reduced to 3–5 °C. The disproportionate lengthening of this second plateau at salinities

above 5% is thus explained by the greater brine volume and the smaller driving temperature difference at the eutectic.

4.2 Unconfined compression tests

4.2.1 Unconfined compression tests at -10 °C ambient temperature

After freezing for 24 h, all specimens had completed their freezing process (Figure **3** and **4**). Unconfined compression tests were conducted at –10 °C for NaCl concentrations up to 7.5%. Three tests are presented for each salt concentration. We do not report error bars because all tests yielded very similar results. The deviation between the standard deviation and the mean value is < 6.0 % for the experiments until 5.0 % NaCl. For 7.5 % NaCl the deviation is 9.1 %. Higher concentrations could not be tested due to insufficient specimen strength as too much UWC was present.

Figure **5** shows the mean peak stresses from the tests. The most significant reduction in strength occurs already at very low salt contents. The specimen with 0.5% NaCl exhibits only about 25% of the peak stress of the reference specimen (0.0% NaCl). From this point onward, the reduction is approximately linear with increasing salinity, although local deviations (e.g., at 3.5–4.0% NaCl) are observed.

These results confirm earlier findings by Jagow-Klaff (2001), who reported that at –10 °C, a specimen with 3.0% NaCl had only ~20% of the strength of a salt-free specimen. The disproportionate loss of strength at very low salt contents highlights the sensitivity of frozen soil strength to even minor salinity, which can be explained by the high unfrozen water content relative to ice bonding at this temperature (Watanabe & Mizoguchi, 2002; Tilston et al., 2010).

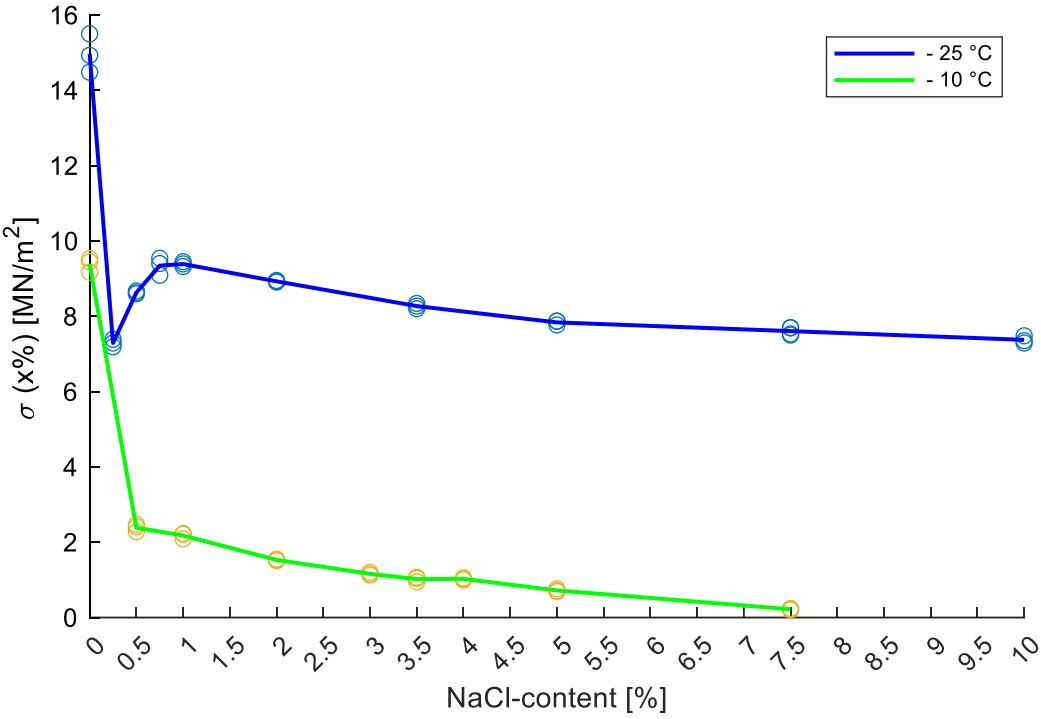

Fig. 5. Mean failure stresses of uniaxial compression tests at -10 °C and -25 °C for different NaCl contents. The dots show the three repetitions at each salt content.

4.2.2 Unconfined compression tests at -25 °C ambient temperature

At –25 °C, specimens were fully frozen, including the residual eutectic brine. Figure **5** shows the mean peak stresses as a function of NaCl concentration (0–10%). Again, three tests are presented for each salt concentration. The deviation between the standard deviation and the mean value < 1.3 % for the experiments containing NaCl. For 0.75 % NaCl the deviation is 2.5 %. The deviation for the reference sample (0% NaCl) is 3.4 %. This is justified by the usage of the 10-t load cell instead of the 2-t load cell for the measurement of the reference sample.

The reference sample (0% NaCl) exhibited significantly higher strength than at –10 °C, reflecting the stronger, more continuous ice matrix at lower temperature. Interestingly also, strength does not decrease monotonically with salinity. At low concentrations (up to 0.25% NaCl), strength decreases, but between 0.25% and 1.0% NaCl, strength partially recovers, forming a plateau before declining again exponentially with higher salinity.

We hypothesise that this non-linearity is caused by microstructure effects. At –25 °C, essentially all pore water is frozen, but at very low salinity (<0.5%), brine channels can still weaken intergranular bonding by creating micro-defects during freezing. At slightly higher salinity (~0.5–1.0%), the segregated salt crystals or solidified brine pockets may “fill in” voids and act as local stiffeners, giving a temporary plateau in strength. Instead of isolated defects, there is a “packing effect” where salt precipitates partly stabilize the skeleton. Hence, the sharp strength drop halts, and you see a temporary plateau or partial recovery in the stress curve. At higher salinities (>1–2%), the increasing fraction of salt crystals incorporated into the matrix weakens the ice skeleton again because inclusions become too abundant, interrupting the continuity of the ice bonds. Instead of reinforcing, they act as weak, brittle inclusions within the ice–soil matrix. Strength therefore decreases again, now in a more systematic exponential fashion with salinity. A further factor affecting this hypothesis is that we observed that SC2 crystals show a semi-viscous behaviour (as a sludge) rather than Ice Ih that is harder and more brittle. This interplay also contributes to the above hypothesis, as SC2 is clearly stronger than liquid brine, but softer than Ice Ih. This will be further investigated in future work.

If we normalize the peak stresses (Figure **6**) of the experiments at -10 °C and -25 °C to the respective reference samples with 0 % NaCl strength is reduced about 50 % highest at -25 °C. This is a significant difference to the observations at -10 °C where the smallest observed amount of NaCl (0.5 %) decrease the strength to a value of about 25 % of the reference sample.

4.3 NMR testing for determining the amount of liquid phase at -10 °C

To directly measure the UWC, additional tests were performed using nuclear magnetic resonance (NMR).

All NMR relaxation measurements presented in this work are conducted with a low field Halbach NMR spectrometer with a frequency of 3.91 MHz (Halbach, 1980; Anferova et al. 2007) using the Carr-Purcell-Meiboom-Gill (CPMG) pulse sequence (Carr & Purcell, 1954;

Meiboom & Gill, 1958). The shortest possible echo time in our setup is TE = 320 µs and, depending on the saturation and relaxation behavior of the corresponding sample, up to 2500 echoes were recorded, yielding signal lengths up to 0.8 s. Initially, each CPMG echo train was averaged until a signal-to-noise ratio of S/N~200 was reached. Details about the measurement procedure can be found in the Appendix.

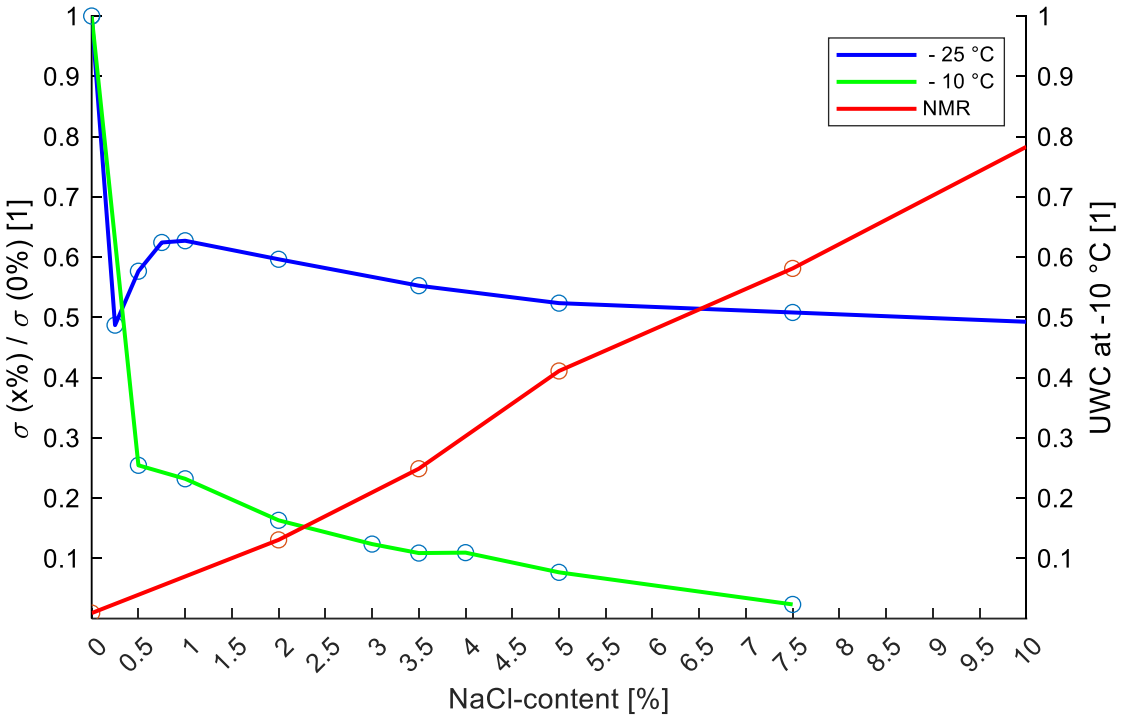

Fig. 6. To 0 % NaCl normalized mean failure stresses at -10 °C and -25 °C and determination of the liquid phase related to the pore-volume with NMR at -10 °C for different NaCl contents

The results (Figure **6**) show that the fraction of unfrozen liquid increases nearly linearly with salinity. At 10% NaCl, approximately 80% of the pore water remained liquid at –10 °C, leaving only 20% frozen.

The NMR measurements of unfrozen water content at –10 °C align well with predictions from the NaCl–H_2O phase diagram when the lever rule is applied. In a binary ice–brine system, the lever rule gives the relative proportions of the two phases at a given bulk concentration C and temperature T:

$$f_{\text{liq, ideal}}(C,T) = \frac{C - C_{\text{sol}}(T)}{C_{\text{liq}}(T) - C_{\text{sol}}(T)}$$

where

- $f_{\text{liq, ideal}}$ is the theoretical liquid (brine) fraction,
- C is the bulk NaCl concentration,
- $C_{\text{sol}}(T)$ is the solidus composition (ice boundary),
- $C_{\text{liq}}(T)$ is the liquidus composition (brine boundary).

However, even salt-free specimens retain a small liquid fraction due to pore-scale forces (e.g. van der Waals interactions). NMR tests on the 0% NaCl sample indicated ~1% residual liquid water. To account for this, the corrected liquid fraction is expressed as:

$$f_{\text{liq}}(C,T) = f_{\text{liq, ideal}}(C,T) + 0.01$$

Comparison of this corrected lever rule with NMR results (Table 2) shows excellent agreement up to about 5% NaCl. At higher concentrations, deviations become larger, likely due to pore-scale effects and salt redistribution not captured by the idealized phase diagram. This highlights important areas of future research.

At –25 °C, the system enters the ice + NaCl·2H_2O (SC2) stability field, and the coexisting liquid fraction predicted by the lever rule tends to zero (apart from the residual 0.01). This corresponds to the second plateau observed in the freezing curves (Figure 4).

Comparing these NMR results with the unconfined compression tests reveals a nonlinear strength–liquid relationship: the largest relative strength loss occurs already at very low salt concentrations, while further increases in liquid fraction reduce strength more gradually. This suggests that factors beyond liquid fraction alone — such as microstructural disruption of the ice–soil matrix — contribute significantly to strength reduction at low salinities (Arenson & Sego, 2004; Luo et al., 2023).

Table 2. Calculated liquid phase by lever-rule approach and measured liquid phase by NMR.

$\%\ NaCl$	$f_{\text{liq, ideal}}(C,T)$	$f_{\text{liq}}(C,T)$	**NMR results**
0.5	0.033	0.043	-
1.0	0.067	0.077	-
2.0	0.133	0.143	0.131
3.5	0.233	0.243	0.249
5.0	0.333	0.343	0.411
7.5	0.500	0.510	0.581
10.0	0.667	0.677	0.783

5 Conclusions

This study provides one of the few systematic experimental datasets that combine freezing curve measurements and mechanical strength testing of saline sands, interpreted within the framework of the NaCl–H_2O phase diagram. While freezing point depression of saline soils is well known, the disproportionate reduction in strength at very low salinities and the partial recovery at eutectic conditions represent new insights into the coupled thermodynamic and mechanical behaviour of frozen soils. These findings extend classical knowledge and have direct implications for artificial ground freezing and permafrost engineering. The results presented here are limited to a narrow-graded, fully saturated sand tested with NaCl solutions at two ambient temperatures and a fixed strain rate, and should not be directly extrapolated to soils containing fines, other pore-water chemistries, or different loading conditions without caution

The main conclusions are as follows:

1. Increasing NaCl content systematically reduced both the supercooling temperature (T_{SC}) and equilibrium freezing point (T_f). The observed freezing curves agree with the NaCl–H_2O phase diagram (Journaux et al., 2023) and confirm that brine remains

liquid above the eutectic temperature of –21.15 °C. A simple lever rule confirms this and provides a simple, initial, way to quantify UWC.

2. At –25 °C, specimens exhibited a second plateau in the cooling curves, corresponding to eutectic freezing of residual brine. The duration of this plateau increased disproportionately for concentrations above 5%, consistent with salt precipitation kinetics.
3. At –10 °C, even 0.5% NaCl reduced strength to ~25% of the salt-free reference value, confirming the disproportionate sensitivity of frozen soil strength to minor salinity. This effect is explained by the high unfrozen water content relative to ice bonding.
4. At –25 °C, residual brine solidified, restoring ice continuity and resulting in higher overall strength. A temporary strength plateau between 0.25% and 1.0% NaCl suggests that salt crystallization may partially stabilize the matrix before higher salinities cause further strength loss. A microstructural plus crystal form explanation is provided but yet needs to be validated.
5. NMR results showed a nearly linear increase in unfrozen brine with salinity at –10 °C, reaching ~80% liquid at 10% NaCl. However, the strength–liquid relation was nonlinear: the greatest relative strength loss occurred at low salinities, indicating that microstructural disturbance of the ice–soil skeleton is as important as liquid fraction alone.
6. For artificial ground freezing and saline permafrost, even low salinities can significantly compromise frozen soil strength at moderate subzero temperatures. At lower temperatures approaching the eutectic, strength partly recovers, but the presence of embedded salt crystals results in a different mechanical response than in salt-free soils. Design must therefore consider both freezing temperature depression and strength loss, with site-specific calibration for salinity.

Acknowledgements

We sincerely thank the laboratory team of GUT for their excellent and reliable assistance. Special thanks to Prof. Dr. Norbert Klitzsch of the Institute for Applied Geophysics and Geothermal Energy to enable the use of their NMR device at the E.ON ERC laboratory.

References

Amankwah, S. K., Ireson, A. M., Maulé, C., Brannen, R., & Mathias, S. A. (2021). A model for the soil freezing characteristic curve that represents the dominant role of salt exclusion. *Water Resources Research*, 57(8), e2021WR030070.

Andersland, O. B., & Ladanyi, B. (2004). *Frozen ground engineering*. John Wiley & Sons.

Anferova, S., Anferov, V., Arnold, J., Talnishnikh, E., Voda, M. A., Kupferschläger, K., ... & Blümich, B. (2007). Improved Halbach sensor for NMR scanning of drill cores. *Magnetic resonance imaging*, 25(4), 474-480.

Arenson, L. U., & Sego, D. C. (2004). Freezing processes for a coarse sand with varying salinities. In *Proceedings of the Cold Regions Engineering & Construction Conference, Edmonton, Alta* (Vol. 16719).

Atkins, P. W. (1996). Physikalische Chemie, 2. Auflage. VCH.

Banin, A., & Anderson, D. M. (1974). Effects of salt concentration changes during freezing on the unfrozen water content of porous materials. *Water Resources Research*, 10(1), 124-128.

Carr, H. Y., & Purcell, E. M. (1954). Effects of diffusion on free precession in nuclear magnetic resonance experiments. *Physical review*, 94(3), 630-638.

Gao, X., Tian, R., Jiang, Y., Guo, Z., & Lei, L. (2024). Frozen saline sand can be highly permeable. *Geophysical Research Letters*, 51(19), e2024GL111946.

Haghighi, H., Chapoy, A., & Tohidi, B. (2008). Freezing point depression of electrolyte solutions: experimental measurements and modeling using the cubic-plus-association equation of state. *Industrial & engineering chemistry research*, 47(11), 3983-3989.

Halbach, K. (1980). Design of permanent multipole magnets with oriented rare earth cobalt material. *Nuclear instruments and methods*, 169(1), 1-10.

Jessberger, H., & Jagow-Klaff, R. (2001). Bodenvereisung. *Grundbau-Taschenbuch, Teil 2: Geotechnische Verfahren*, S. 121-166.

Journaux, B., Pakhomova, A., Collings, I. E., Petitgirard, S., Boffa Ballaran, T., Brown, J. M., ... & Hanfland, M. (2023). On the identification of hyperhydrated sodium chloride hydrates, stable at icy moon conditions. *Proceedings of the National Academy of Sciences*, 120(9), e2217125120.

Ju, Z., Lu, S., Guo, K., & Liu, X. (2023). Changes in the thermal conductivity of soil with different salts. *Journal of Soils and Sediments*, 23(9), 3376-3383.

Loomis, E. H. (1896). On the freezing-points of dilute aqueous solutions. *Physical Review (Series I)*, 3(4), 270.

Luo, C. L., Yu, Y. Y., Zhang, J., Tao, J. Y., Ou, Q. J., & Cui, W. H. (2023). Thermal-water-salt coupling process of unsaturated saline soil under unidirectional freezing. *Journal of Mountain Science*, 20(2), 557-569.

Meiboom, S., & Gill, D. (1958). Modified spin-echo method for measuring nuclear relaxation times.

Mitchell, J., Webber, J. B. W., & Strange, J. H. (2008). Nuclear magnetic resonance cryoporometry. *Physics Reports*, 461(1), 1-36.

Orth, W., Solf, O., Perl, C. & Rizos, D. (2021). *STUVA Conference 2021, Karlsruhe*. ISBN 978-3-00-070615-8.

Rizos, D., Orth, W., Perl, C., Solf, O., Eramo, N. & Amin, T. (2022). Port Said Tunnels under the Suez Canal - Cross passages with ground freezing in aggressive conditions. *In Proceedings of the World Tunnel Congress (WTC). Copenhagen*: ITA Bookshop. ISBN 978-2-9701436-7-3

Tilston, E. L., Sparrman, T., & Öquist, M. G. (2010). Unfrozen water content moderates temperature dependence of sub-zero microbial respiration. *Soil Biology and Biochemistry*, 42(9), 1396-1407.

Wan, X., Lai, Y., & Wang, C. (2015). Experimental study on the freezing temperatures of saline silty soils. *Permafrost and Periglacial Processes*, 26(2), 175-187.

Wan, X., Liu, E., & Qiu, E. (2021). Study on ice nucleation temperature and water freezing in saline soils. *Permafrost and Periglacial Processes*, 32(1), 119-138.

Wan, X., Zhu, J., Lai, Y., Lu, J., & Yan, Z. (2024). Premelting theory-based mechanism for water freezing in saline soil. *Water Resources Research*, 60(10), e2024WR038013.

Wang, C., Li, K., Cai, H., Wu, Y., Lin, Z., & Li, S. (2023). Study of Supercooling Phenomena in Soil-Water Systems Based on Nucleation Theory: Quantifying Supercooling Degree. *Water Resources Research*, 59(11), e2023WR035935.

Watanabe, K., & Mizoguchi, M. (2002). Amount of unfrozen water in frozen porous media saturated with solution. *Cold Regions Science and Technology*, 34(2), 103-110.

Xiao, Z., Lai, Y., & Zhang, M. (2018). Study on the freezing temperature of saline soil. Acta *Geotechnica*, 13, 195-205.

Ying, S., Cao, Y., Zhang, Q., Xia, X., Li, G., Zhou, F., & Wen, T. (2025). The effect of salt on the freezing temperature of saline soil. *Soils and Foundations*, 65(1), 101566.

Zhou, J., Wei, C., Lai, Y., Wei, H., & Tian, H. (2018). Application of the generalized Clapeyron equation to freezing point depression and unfrozen water content. *Water Resources Research*, 54(11), 9412-9431.

APPENDIX A - NMR measurements

For measurement purposes, samples with an inner diameter of 2.7 cm (outer diameter 3.0 cm) and a height of 5.5 cm were prepared in sealed glass tubes as recommended by Mitchell et al. (2008). This maintained a ratio of 1:2 again. Subsequently, the samples were frozen at -10 °C. A saturated NaCl solution without sand was also prepared to serve as a reference during measurement.

To carry out NMR measurements first, washers had to be placed in the NMR device to bring the sample to the correct height. The NMR device has a sensitive measuring range between heights of 70 mm and 100 mm and a highly sensitive range between 80 mm and 90 mm. Since the sample had a height of 55 mm, it was raised by adding spacers up to 60 mm beneath it. Thus, the centre of the sample lay within the sensitive measuring range. Subsequently, fine-tuning of excitation frequency was performed since it should have a value of 3.91 MHz for accurate measurement results

The measurement process for a sample proceeded as follows:

1. Measure temperature
2. NMR measurement of reference sample NaCl without sand
3. Measure temperature
4. NMR measurement of sand sample
5. Measure temperature
6. NMR measurement of reference sample NaCl without sand
7. Measure temperature

Temperature measurements between NMR measurements were necessary because during NMR measurements, cooling had to be switched off. Otherwise, electrical frequencies emitted by the freezer would disturb measurements. Each measurement took approximately half an hour during which time temperatures in the freezer increased by up to a maximum of 0.9 °C during measurement periods.

To obtain meaningful reference measurements, averages from reference measurements before and after measuring sediment samples were calculated so that any temperature difference occurring during these measurements could be corrected.